Topological states in Bi_2Se_3 surfaces created by cleavage within a quintuple layer: Analysis in terms of the Shockley criterion

Xiaoxiong Wang[1,*] and T.-C. Chiang[2,3,4,†]

[1]*College of Science, Nanjing University of Science and Technology, Nanjing 210094, China*

[2]*Department of Physics, University of Illinois at Urbana-Champaign, 1110 West Green Street, Urbana, Illinois 61801-3080, USA*

[3]*Frederick Seitz Materials Research Laboratory, University of Illinois at Urbana-Champaign, 104 South Goodwin Avenue, Urbana, Illinois 61801-2902, USA*

[4]*Synchrotron Radiation Center, University of Wisconsin-Madison, 3731 Schneider Drive, Stoughton, Wisconsin 53589-3097, USA*

(Received 10 January 2014; revised manuscript received 27 February 2014; published 14 March 2014)

In topologically trivial materials, the existence of surface states within the bulk band gap depends on the surface condition. A surface state exists if the system is Shockley inverted, and vice versa; furthermore, this surface condition in a superlattice can be tuned from one case to the other by varying the terminating atomic plane within a superlattice period. By contrast, we demonstrate here based on first-principles calculations for Bi_2Se_3 cleaved at different atomic planes within a quintuple layer that topological surface states always span the bulk band gap in accordance with the topologically nontrivial nature of Bi_2Se_3. However, the number of surface bands, the band dispersion relations, and the degree of spin polarization are strongly dependent on the cleavage plane. Multiple Dirac cones can exist at the zone center and/or zone boundary, and a massive but topologically nontrivial Dirac cone is observed for a Se-terminated surface. The results confirm the robustness of the topological nature of the system, but the details of the topological surface states themselves can vary substantially within the broad topological constraint. The persistent existence of topological states within the gap is discussed in terms of the Shockley criterion.

DOI: 10.1103/PhysRevB.89.125109 PACS number(s): 73.20.At, 73.22.−f

I. INTRODUCTION

Topological insulators [1–3], especially three-dimensional ones [4], have attracted much interest for their unusual boundary properties that promise technological applications in spin information processing [1]. The topological insulator has a finite charge excitation energy gap in its interior but possesses gapless surface or edge states [5,6]. Due to a strong spin-orbit coupling in these materials, the band gap is inverted; namely, the conduction and valence band edges with opposite parities switch their relative energy positions with this relativistic effect taken into account [5]. The inverted band gap makes the band structure topologically distinct from ordinary insulators [7]. This distinction is a bulk property and is thus insensitive to perturbations at the boundaries. This insensitivity is often referred to as "protection" by time-reversal symmetry [1]. An important consequence of the gap inversion is that the boundaries of topological insulators, or interfaces with a vacuum (a trivial insulator), are always metallic [5,7]. Thus, the bulk gap is always spanned by surface states. The strong spin-orbit coupling makes the surface states highly spin polarized owing to the Rashba effect [8,9]. These qualitative features, being topologically protected, are of interest to spintronic applications [10] and quantum topological computation [11]. For systems with spatial inversion symmetry, such as Bi_2Se_3, the topological order can be determined by counting the Fermi level crossings of surface bands between two neighboring time-reversal-invariant momenta in the Brillouin zone; an odd number of crossings corresponds to a topologically nontrivial case, and vice versa [12].

By contrast, topologically trivial insulators may or may not have surface states within the bulk band gap. For example, dangling bonds on semiconductor surfaces often give rise to surface states that can be readily modified or eliminated by surface adsorption or passivation [13–15]. Free-electron-like metals can also support surface states in a relative band gap if and only if the gap is Shockley inverted, where a Bloch state inside the metal with a complex wave vector can be matched to an exponentially decaying wave in a vacuum [16,17]. A free-electron-like metallic superlattice can likewise support surface states; furthermore, the surface condition can be systematically varied by choosing different terminating atomic planes within a superlattice period [18]. In general, a surface state exists only for one half of the superlattice period of terminating plane variation. Therefore, a randomly selected terminating atomic plane for a superlattice has a 50% chance of having a surface state.

Here, we investigate by theoretical computation a related question: What happens to the topological surface states when a layered topological insulator, such as Bi_2Se_3, is cleaved to expose various atomic planes? This material has a layered structure made of quintuple layers (QLs), where each quintuple is made of two Bi atomic layers intercalated in three Se atomic layers [5]. The bonding within each QL is largely covalent, while the inter-QL bonding is of the van der Waals type. The crystal usually cleaves between neighboring QLs, but intra-QL cleavage has been observed over limited areas by scanning tunneling microscope (STM), where the local electronic structure has been measured and compared with calculated band structure [19]. This observation and analysis motivate our further work on this system.

By peeling away one atomic layer at a time from the QL-terminated surface, the same surface is recovered after the

*phywangxx@njust.edu.cn

†tcchiang@illinois.edu

removal of five atomic layers. Generally, we can expect the surface states to go through periodic variations with a period of five atomic layers, and our study focuses on the detailed variations, including the band structure and the charge and spin distributions of the surface states. These issues are of interest in view of the topological constraint that requires the existence of topological surface states no matter what the surface condition [1,2]. This constraint, however, is quite broad and does not provide further specifics for the surface states. Our studies reveal a rich behavior, with some of the surfaces exhibiting multiple surface bands with massless or massive Dirac cones. The results illustrate some general consequences of the topological order and suggest possible routes for materials optimization based on surface engineering. The connection between the topological constraint and the Shockley criterion, with the latter being independent of spin-orbit coupling, is addressed.

II. COMPUTATIONAL METHODS

The topological insulator Bi_2Se_3 has the rhombohedral R-3m crystal structure made of QL stacks [5]. The unit cell of bulk Bi_2Se_3 is shown in Fig. 1(a). Each unit cell consists of 3 QLs along the $\boldsymbol{c}$ direction. Our starting model is a Bi_2Se_3 slab of 12 QLs. This is much thicker than the minimum thickness of 6 QL needed for the surface states to be essentially in the bulk limit [8,20,21]. The different surface atomic plane terminations within a QL are obtained by removing one atomic layer at a time from each of the two faces of the slab until the film thickness is reduced to 10 QLs. The system retains spatial inversion symmetry throughout the thinning process. The band structure is computed for each case using the Abinit package [22,23] within the local density approximation based on the Teter–Pade parameterization [24]. A supercell geometry with a 15-Å vacuum gap is employed; interactions between neighboring slabs are negligible with this large gap. The wave functions are expanded in terms of plane waves. The cutoff energy is chosen to be 400 eV, and sampling in k-space is done over an $8 \times 8 \times 1$ grid using the Monkhorst–Pack scheme [25]. Relativistic corrections including spin-orbit coupling are taken into account by using the Hartwigsen-Goedecker-Hutter (HGH) pseudopotential [26]. For straightforward comparison of the surface-termination effect, surface relaxation is not included for the results to be presented below. Additional calculations including surface relaxation yield very similar results, but these are not presented here for simplicity. The possibility of surface reconstruction is not considered here.

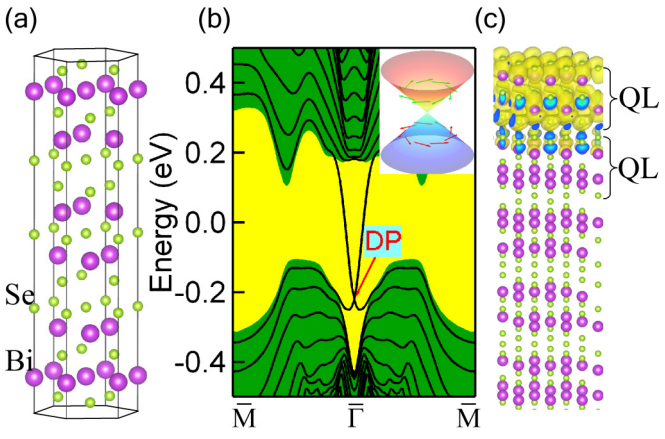

FIG. 1. (Color online) (a) Unit cell of Bi_2Se_3 consisting of three stacked QLs. (b) Band structure of a 10-QL Bi_2Se_3 slab. The green areas indicate the projected bulk continua, while the yellow area indicates the band gap. The energy zero is set at the midpoint of the gap. The inset shows a three-dimensional enlarged view of band structure near the Dirac point (DP). The arrows indicate the spin orientation. (c) The charge density of a state near the DP; it is mostly concentrated within the topmost QL.

III. RESULTS AND DISCUSSION

A. Band Structure Evolution

For reference, the band structure of a 10-QL Bi_2Se_3 slab is shown in Fig. 1(b). The projected bulk band continua are indicated by green shading, and the fundamental gap is indicated by yellow shading. The energy zero is fixed at the midpoint of the bulk band gap. Within the gap, there is a pair of surface states forming a Dirac point (DP) at the zone center. The inset in Fig. 1(b) shows an enlarged view of the surface band dispersions near the DP, where the arrows indicate the direction of spin polarization. The chiral character of the spin orientation is evident [27]. The band dispersion relation near the DP is given by [28]

$$E = c\hat{\mathbf{z}} \cdot \boldsymbol{\sigma} \times \mathbf{k}, \tag{1}$$

where c is the group velocity, $\boldsymbol{\sigma}$ is the Pauli matrix vector, and $\mathbf{k}$ is the wave vector. The value of c is 3.8 eVÅ for 10-QL Bi_2Se_3. The three-dimensional charge density of a surface state very close to the DP is shown in Fig. 1(c). Most of the charge density is concentrated within the top QL of the slab.

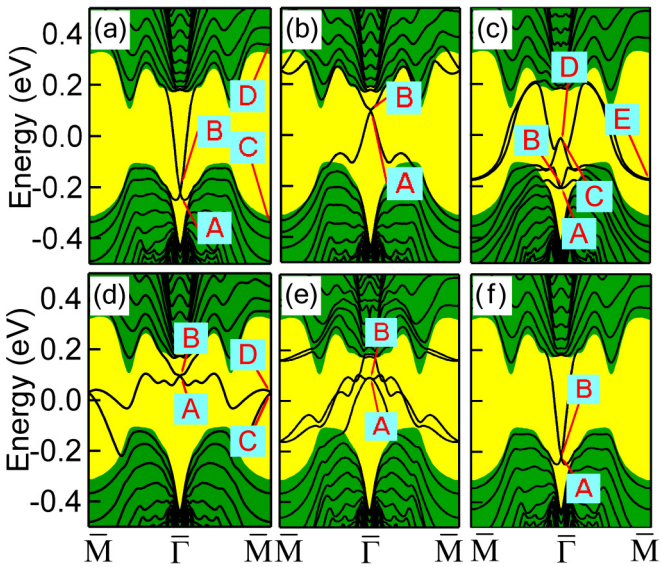

FIG. 2. (Color online) Band structures of Bi_2Se_3 slabs cleaved at different atomic planes in a QL starting from (a) a 12-QL slab to (b)–(f) the same with successive outermost atomic layers peeled away from each side of the slab. The final configuration (f) corresponds to a 10-QL slab. Some states of interest are indicated.

Figure 2(a) shows the corresponding results for a 12-QL slab. Figures 2(b)–2(f) show the results after successively removing the outermost atomic layer from each face of the slab. The final system corresponds to a 10-QL slab [Fig. 2(f)]. The surface band dispersions for the 10- and 12-QL slabs are indistinguishable to the eye, confirming our earlier statement that the surface states at these thicknesses are essentially in the bulk limit.

With the outermost Se atomic layers removed from the 12-QL slab to expose a Bi-terminated surface [Fig. 2(b)], the DP moves up in energy from below the valence band maximum to near the conduction band minimum. This movement or implied control of the DP position can be quite useful for device applications; overlapping of the DP with the valance states in energy, as is the case for the QL-terminated surface, is generally undesirable because the bulk conduction channel can lead to a "leakage" current. Independent tuning of the DP and the Fermi level would be ideal for tailoring the device performance. The Dirac cone now shows considerable distortion, and the dispersion relation is best described by

$$E = c\hat{\mathbf{z}} \cdot \boldsymbol{\sigma} \times \mathbf{k}(1 + \alpha k^2), \tag{2}$$

where α is an expansion coefficient. A fitting gives the parameters of c 0.43 eVÅ and α 43.1 Å^2.

With the further removal of the Bi atomic layer from each of the two faces of the slab, the system is again Se terminated [Fig. 2(c)]. The DP resumes its original position (indicated by states A and B), but the nonlinear dispersion effect is very much enhanced. Furthermore, the two branches of the surface states both connect to the valence band region, instead of spanning the bulk gap; thus, these states associated with the DP become topologically trivial. A new pair of surface states at the zone center is found at about midgap (labeled C and D). These surface states can be attributed to the $4p$ atomic orbitals of the top Se atomic layer for which the chemical valence is not balanced. They cross the zone center but do not form a cone-like dispersion. Instead, the dispersion close to the zone center is best described by

$$E = \frac{\hbar^2 k^2}{2m^*}, \tag{3}$$

where m^* is the effective mass, and the spin-dependent Rashba splitting is zero to first order [29]. The effective mass m^* values for states C and D are $-0.83\ m_e$ and $-0.92\ m_e$, respectively, where m_e is the rest mass of the electron. For simplicity, we refer to the crossing point at the zone center as a "massive Dirac cone." The two surface state branches connected to this massive Dirac cone span the band gap, and thus these states are "topological." There is also a massive Dirac cone at the zone boundary. Despite the complicated appearance of the surface states, the system is topologically nontrivial, as the number of Fermi level crossings by the surface states between $\bar{\Gamma}$ and $\bar{M}$ is odd (3 or 5, depending on the choice of the Fermi level) [12].

By removing yet another layer of Se atoms from each face of the slab, the system becomes Bi-terminated again [Fig. 3(d)]. There is just one Dirac cone at the zone center, very much like the case in Fig. 3(b). As before, band distortion is pronounced. There is also a Dirac cone at the zone boundary. The number of Fermi level crossings remains odd, and the system remains topologically nontrivial.

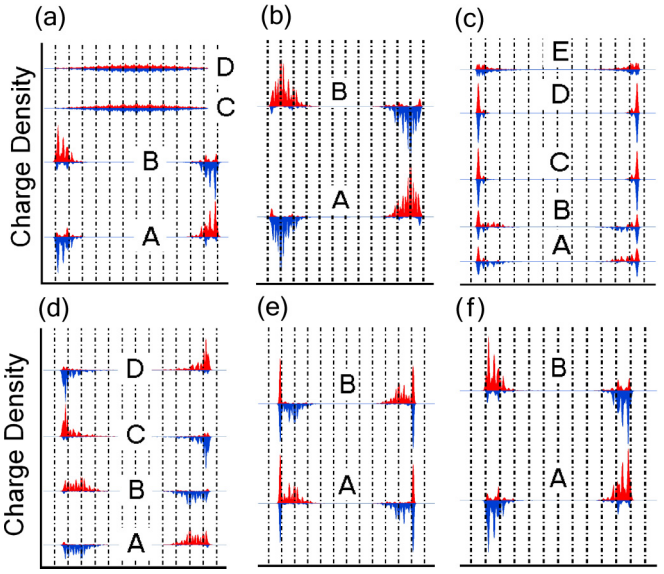

FIG. 3. (Color online) Spin-resolved planar charge density of the states indicated in Fig. 2. The panels are organized in the same order as Fig. 2. Red (blue) filled curves represent the + and − spin components of the charge density.

With the further removal of the top Bi layers, the system becomes Se-terminated again [Fig. 2(e)]. The band structure becomes quite complex. However, there is just one massive Dirac cone at the zone center within the band gap, but the two branches of the surface states do not span the bulk gap. Instead, another surface state band connects to the conduction band region and makes the system topologically nontrivial. By extrapolation, one could argue that this surface band should form a Dirac cone within the conduction band region, but the cone itself is no longer readily identifiable by hybridization with the bulk states.

After a whole QL is removed from each side of the slab, the system returns to the QL-terminated case [Fig. 2(f)]. The surface band structure becomes simple again. The complexity of the band structure for the other cases can be attributed to dangling bonds on the surface that are partially occupied and must (partially) appear in the bulk band gap.

B. Spin-Resolved In-Plane Charge Density Distributions

To further characterize the surface states, the spin-resolved charge density of selected states, as labeled in Fig. 2, is calculated and presented in Fig. 3, with the panels organized in the same order as in Fig. 2. The spin-resolved charge density is defined by

$$\rho^{\pm}(k_x, z) = \int\int \sum_i |\langle \pm |\ \psi_i(k_x, \mathbf{r})\rangle|^2 dx dy, \tag{4}$$

where $|\pm\rangle$ denotes the eigenstates of σ_y, and the summation is over each pair of spin degenerate states. For the selected states near the zone center (boundary), the crystal momentum k_x is set to be 0.033 $\bar{\Gamma}\bar{M}$ (or 0.967 $\bar{\Gamma}\bar{M}$). The slight offset from the zone center or boundary is to avoid the fourfold degeneracy of a DP. All of the electronic states in the system are doubly degenerate because of the spatial inversion symmetry. For the surface

states, the spin degenerate pair is spatially separated, with one state localized at each face of the slab, resulting in a spin separation. For the bulk states, the pair forms spin-unpolarized quantum well states [30].

The vertical dashed lines in Fig. 3 indicate the boundaries of the QLs. Red and blue curves indicate the + and − spin components of the charge density. Figure 3(a) illustrates the surface character and spin separation of topological surface states A and B in a 12-QL slab. Note that these two states are strongly spin polarized, but the degree of polarization is less than 100%, which is expected because of the spin-orbit coupling [8]. For quantum well states C and D, the charge density spreads throughout the film and exhibits no spin imbalance; in other words, these states are spin unpolarized [30]. The results in Fig. 3(b) can be similarly interpreted. The topological surface states A and B are pushed inward into the slab by about a half QL, and so the charge distribution for each state is roughly centered about the boundary between the first and second QLs.

The charge density plots in Fig. 3(c) for the Se-terminated surface show interesting new features. States C and D associated with the nontrivial massive Dirac cone at the zone center are dominated by a sharp peak at the surface Se atomic plane. A detailed analysis shows this peak arises from the Se $4p_x \pm i4p_y$ atomic orbitals. The spin-orbit coupling or Rashba splitting is zero to first order, thus giving rise to a massive fermion dispersion [29]. These states are nearly spin unpolarized. States A and B also consist of a sharp Se $4p$ peak, but there is additionally a substantial tail into the top QL, which gives rise to the observed Rashba splitting. The charge distribution suggests a hybridization interaction between the Se $4p$ and the surface states. The resulting states A and B have a relatively weak spin polarization.

The charge density distributions in Fig. 3(d) can be interpreted similarly. States A and B can be attributed to the topological surface states being moved up in energy due to Bi termination. The charge densities are strongly spin polarized and bear similarities to those shown in Fig. 3(b). For Fig. 3(e), the surface is Se terminated, and all surface states show a sharp peak associated with the Se $4p$ orbitals.

C. Three-Dimensional Charge Distributions

The different nature of the various surface states is further illustrated by the three-dimensional charge density plots presented in Fig. 4 for a few selected states as labeled at the bottom of each panel. Figures 4(a)–4(c) correspond to states B, D, and E, respectively, in Figs. 2(c) and 3(c). The surface is Se-terminated. States B and D show a strong Se $4p_{x,y}$ component associated with the surface Se atoms, but state D alone shows very little charge density within the substrate; its Rashba splitting is zero to first order. The state is largely spin unpolarized, but the surface band is topologically nontrivial (spanning the gap). State E contains a component of the Se $4p_z$ orbital, but the charge density is dominated by a long tail into the substrate. Figures 4(d) and 4(e) correspond to states B and D, respectively, in Figs. 2(d) and 3(d). The surface is Bi-terminated. Both states show a charge distribution decaying into the bulk of the substrate with a decay length of about 1–2 QLs typical of topological surface states.

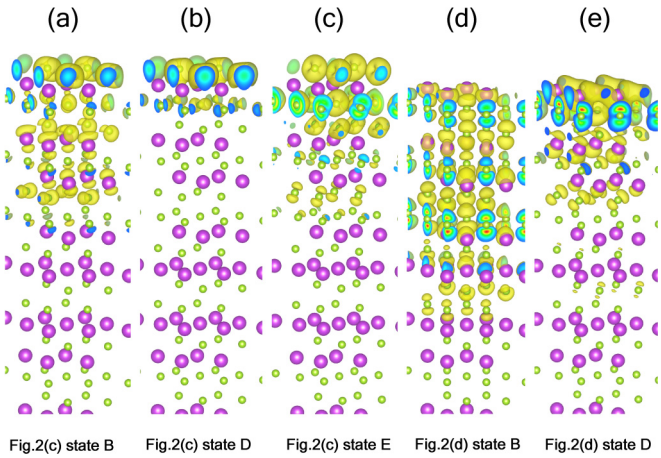

FIG. 4. (Color online) Three-dimensional charge density plots of selected states as labeled at the bottom of each panel.

D. Without Spin-Orbit Coupling

With the spin-orbit coupling in the calculation artificially turned off, the system becomes topologically trivial. All states remain doubly degenerate, but any spin separation or Rashba splitting (for the topological surface states) vanishes. The resulting band structures for the differently terminated slabs are shown in Fig. 5, organized in the same order as that of Fig. 2. With full-QL termination [Figs. 5(a) and 5(f)], there are no surface states in the bulk band gap. Surface states exist for the other cases, but they are spin unpolarized and do not span the bulk gap. These surface states can be attributed to the unbalanced chemical valences of the surface atomic layers. It is straightforward to verify that the number of Fermi level crossings of the surface states in each case is always even, in agreement with the topological counting rule.

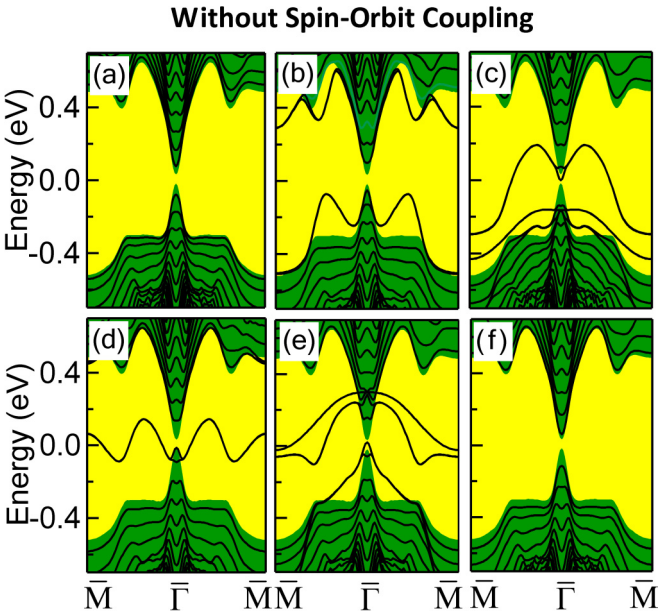

FIG. 5. (Color online) Same as Fig. 2 except that the spin-orbit coupling is turned off in the calculation.

There is some vague similarity between the bands in Figs. 5 and 2, and the evolution from one case to the other can be easily followed in the calculation by numerically scaling the strength of the spin-orbit coupling. The results are not shown here for simplicity. For the QL-terminated slabs, increasing the spin-orbit coupling strength starting from 0 to 100% leads to the closure of the band gap at the zone center at 31% coupling strength, beyond which the gap at the zone center reopens but with inverted parities [31]. The gap reopening is accompanied by the emergence of a Dirac cone and the corresponding topological surface states, which are originally band-edge states but are now left in the band gap as the gap widens.

For the other surfaces, similar gap closing and reopening occur. Again, a topological state pair emerges after gap reopening, but these states hybridize with the other surface states that are already in the gap to form more complex shapes. The hybridization results in anticrossing, and so the particular bands that span the band gap can exhibit different characters in going from the zone center to the zone boundary.

E. Analysis in Terms of the Shockley Criterion

Bloch state solutions can be found in bulk band gaps of solids with complex wave vectors that give rise to an exponential envelope function. These are unphysical solutions in infinite solids, but they can exist at surfaces. If an exponentially damped Bloch solution in the solid can be matched at the surface to a damped wave in a vacuum, it is a physical solution and corresponds to a surface state. In Shockley's treatment of a free-electron-like material, a surface state exists if the band gap is inverted (referred to as Shockley inverted), thus allowing the wave-function matching condition to be satisfied at an appropriate energy, and vice versa [16,17]. However, the parities of the edge states across the gap actually depend on the choice of the coordinate system [17]. For example, a sine-like odd function becomes a cosine-like even function with the coordinate system shifted by one quarter of a period. The real issue for the Shockley criterion is the location of the effective surface plane (or the plane for wave-function matching) relative to the crystal lattice, which is coordinate independent, rather than the edge-state parity, which is coordinate dependent.

For simplicity, let us consider the Shockley model with his choice of the coordinate system. Assuming that the effective surface plane can be adjusted continuously from one atomic plane to the next, the surface state energy will vary continuously and periodically. In one period, the surface state will move from one edge of the gap to the other edge over a half period, disappear for another half a period, and reappear at the same edge of the gap after one complete period; the phase of the periodic variation is system dependent [18]. Basically, the change in surface plane location leads to a change in phase shift of the matching wave functions, and for half of the period of variation, matching of the wave functions across the surface plane becomes impossible because of the different signs of the logarithmic derivatives. This periodic variation has been experimentally observed in an Ag-Au superlattice [18], where the terminating surface atomic layer can be varied within a superlattice period. The variation is discrete but has enough resolution within a superlattice period to illustrate the surface state evolution.

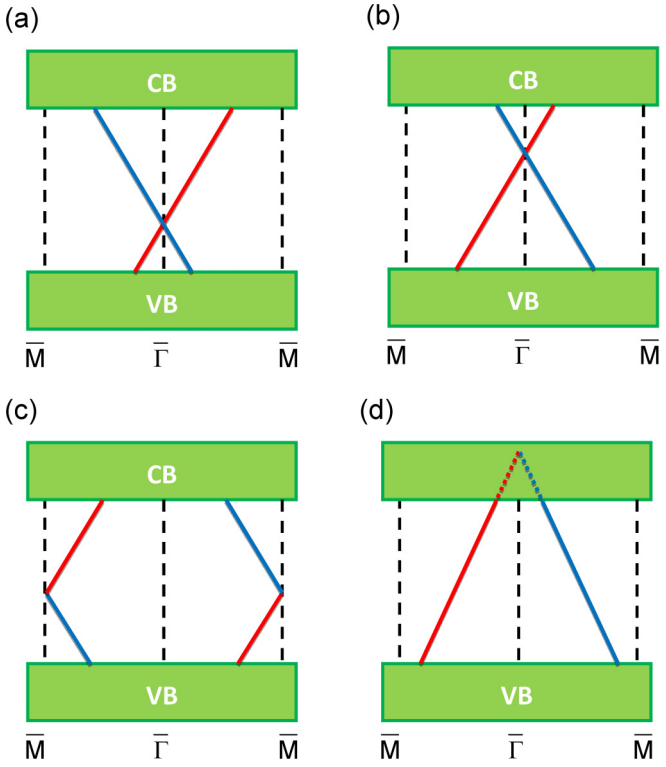

FIG. 6. (Color online) Schematic band diagrams showing various dispersion relations for the topological surface states. The conduction and valence band regions (CB and VB) are shaded green. The red and blue curves represent surface states related by time-reversal symmetry.

The Shockley criterion holds true independent of spin-orbit coupling. How is it connected to the topological constraint on surface states? Let us consider one spin-split component for a simple case without dangling bonds (like the QL-terminated Bi_2Se_3 surface), as represented by the highly schematic diagram in Fig. 6(a). The gap is inverted at the zone center $\bar{\Gamma}$ (with a surface state) but not at the zone boundary $\bar{M}$ (without a surface state). As the wave vector k_x increases from $\bar{M}$ to $\bar{\Gamma}$ and to $\bar{M}$ along the horizontal axis, the character of the gap varies through one cycle, and the phase shift for wave-function matching also goes through one cycle. Based on the Shockley criterion, a surface state should emerge somewhere between $\bar{M}$ and $\bar{\Gamma}$, move continuously across the gap, and merge into the bulk band region somewhere between $\bar{\Gamma}$ and $\bar{M}$, as represented schematically by the red band in Fig. 6(a). Its spin partner (blue band) is obtained by applying time-reversal symmetry, and it appears as a mirror image about the zone center (with k_x changing to $-k_x$). This simple picture illustrates the general qualitative features of the topological surface states in QL-terminated Bi_2Se_3. The quantitative details can be more complicated, however, because the phase shift for wave-function matching can depend on k_x, and the band gap can show considerable variations within the Brillouin zone. Thus, the range in k_x covered by the surface band is not necessarily one half of the distance from

the zone center to the zone boundary, and the surface states can exhibit nonmonotonic dispersion relations.

With different surface terminations of Bi_2Se_3, the phase shift for wave-function matching differs, and the surface bands move sideways correspondingly, as illustrated by the case shown in Fig. 6(b), which corresponds roughly to the Bi-terminated cases with the Dirac cone at a higher energy. More generally, the unsatisfied chemical valences of the surface atomic layers can give rise to additional surface states, which can hybridize with the Shockley states and yield a complex surface band structure.

For completeness, we show in Fig. 6(c) a case where the phase shift is such that the Dirac cone occurs at the zone boundary. Prior theoretical calculations show that this case can be realized in hydrogen-terminated Bi_2Se_3 [32]. Figure 6(d) shows a case where the system does not have a Dirac cone within the gap. One could argue that a Dirac cone exists in the conduction band (or the valence band) by extrapolation, as suggested by the dashed lines. However, anticrossing with bulk states will actually keep the surface states at the band edges.

IV. CONCLUDING REMARKS

Our studies based on first-principles calculations of Bi_2Se_3 cleaved at various atomic planes within a QL yield the following conclusions about the topological surface electronic structure. (1) The system is topologically nontrivial, independent of the cleavage plane, as evidenced by an odd number of Fermi level crossings by the surface states for any Fermi level position within the bulk gap. The gap is always spanned by surface states, and the surface is always metallic. This situation is quite different from the topologically trivial cases, where the surface can be either metallic or insulating. (2) The number of surface state bands and the number of Fermi level crossings can depend strongly on the surface termination. (3) Multiple Dirac cones can occur at the zone center and/or the zone boundary. (4) Some of the Dirac cones can be massive (or with zero Rashba splitting to first order). (5) Se-terminated surfaces created by cleavage within a QL exhibit surface states with a strong Se $4p$ character, and the Rashba splitting is generally weaker than that for the Bi-terminated surfaces. Bi-termination tends to move the Dirac cone up in energy. (6) The degree of spin polarization of the surface states is less than 100% and can vary substantially from case to case. For spin information processing, it is best to work with highly spin-polarized surface states with a large group velocity. The Bi-terminated surfaces seem to be better suited for applications because of the stronger spin polarization and fewer number of Fermi level crossings, leading to less interband scattering.

Finally, the overall features of the surface bands have been analyzed in terms of the Shockley criterion, which has been widely used for analyzing surface states in ordinary materials. For simple topological insulators such as Bi_2Se_3, the topological condition involves an inverted band gap at one time-reversal-invariant point in the Brillouin zone and a noninverted gap at a nearby time-reversal-invariant point. The application of the Shockley criterion shows that there must be a surface band that spans the gap over a part of the Brillouin zone. Different surface terminations can shift the surface bands. Additional surface bands from dangling bonds can arise and hybridize with the topological surface states to yield a complicated band structure.

ACKNOWLEDGMENTS

This work was supported by the US Department of Energy, Office of Science (Grant No. DE-FG02-07ER46383 to T.C.C.), the National Natural Science Foundation of China (Grant No. 11204133 to X.W.), the Jiangsu Province Natural Science Foundation of China (Grant No. BK2012393 to X.W.), and the Young Scholar Project of Nanjing University of Science and Technology (X.W.).

[1] M. Z. Hasan and C. L. Kane, Rev. Mod. Phys. **82**, 3045 (2010).
[2] X.-L. Qi and S.-C. Zhang, Rev. Mod. Phys. **83**, 1057 (2011).
[3] J. E. Moore, Nature **464**, 194 (2010).
[4] M. Z. Hasan and J. E. Moore, Annu. Rev. Condens. Matter Phys. **2**, 55 (2011).
[5] H. Zhang, C. X. Liu, X. L. Qi, X. Dai, Z. Fang, and S. C. Zhang, Nat. Phys. **5**, 438 (2009).
[6] D. Hsieh, Y. Xia, L. Wray, D. Qian, A. Pal, J. H. Dil, J. Osterwalder, F. Meier, G. Bihlmayer, C. L. Kane, Y. S. Hor, R. J. Cava, and M. Z. Hasan, Science **323**, 919 (2009).
[7] L. Fu, C. L. Kane, and E. J. Mele, Phys. Rev. Lett. **98**, 106803 (2007).
[8] O. V. Yazyev, J. E. Moore, and S. G. Louie, Phys. Rev. Lett. **105**, 266806 (2010).
[9] Z. H. Pan, E. Vescovo, A. V. Fedorov, D. Gardner, Y. S. Lee, S. Chu, G. D. Gu, and T. Valla, Phys. Rev. Lett. **106**, 257004 (2011).
[10] S. Raghu, S. B. Chung, X. L. Qi, and S. C. Zhang, Phys. Rev. Lett. **104**, 116401 (2010).
[11] L. Fu and C. L. Kane, Phys. Rev. Lett. **100**, 096407 (2008).
[12] L. Fu and C. L. Kane, Phys. Rev. B **76**, 045302 (2007).
[13] G. P. Srivastava, *Theoretical Modelling of Semiconductor Surfaces: Microscopic Studies of Electrons and Phonons* (World Scientific, Singapore, 1999).
[14] A. Zangwill, *Physics at Surfaces* (Cambridge University Press, Cambridge, 1988).
[15] B. Feuerbacher, B. Fitton, and R. F. Willis, *Photoemission and the Electronic Properties of Surfaces* (Wiley, New York, 1978).
[16] W. Shockley, Phys. Rev. **56**, 317 (1939).
[17] N. V. Smith, Phys. Rev. B **32**, 3549 (1985).
[18] T. Miller and T.-C. Chiang, Phys. Rev. Lett. **68**, 3339 (1992).
[19] H. Lin, T. Das, Y. Okada, M. C. Boyer, W. D. Wise, M. Tomasik, B. Zhen, E. W. Hudson, W. Zhou, V. Madhavan, C.-Y. Ren, H. Ikuta, and A. Bansil, Nano Lett. **13**, 1915 (2013).
[20] C.-X. Liu, H. J. Zhang, B. Yan, X.-L. Qi, T. Frauenheim, X. Dai, Z. Fang, and S.-C. Zhang, Phys. Rev. B **81**, 041307(R) (2010).

[21] H.-Z. Lu, W.-Y. Shan, W. Yao, Q. Niu, and S.-Q. Shen, Phys. Rev. B **81**, 115407 (2010).
[22] X. Gonze *et al.*, Comput. Phys. Commun. **180**, 2582 (2009).
[23] X. Gonze, G.-M. Rignanese, M. Verstraete, J.-M. Beuken, Y. Pouillon, R. Caracas, F. Jollet, M. Torrent, G. Zerah, M. Mikami, P. Ghosez, M. Veithen, J.-Y. Raty, V. Olevano, F. Bruneval, L. Reining, R. Godby, G. Onida, D. R. Hamann, and D. C. Allan, Z. Kristallogr. **220**, 558 (2005).
[24] S. Goedecker, M. Teter, and J. Hutter, Phys. Rev. B **54**, 1703 (1996).
[25] H. J. Monkhorst and J. D. Pack, Phys. Rev. B **13**, 5188 (1976).
[26] C. Hartwigsen, S. Goedecker, and J. Hutter, Phys. Rev. B **58**, 3641 (1998).
[27] P. Roushan, J. Seo, C. V. Parker, Y. S. Hor, D. Hsieh, D. Qian, A. Richardella, M. Z. Hasan, R. J. Cava, and A. Yazdani, Nature **460**, 1106 (2009).
[28] Y. A. Bychkov and É. I. Rashba, JETP Lett. **39**, 78 (1984).
[29] X. Wang, G. Bian, T. Miller, and T.-C. Chiang, Phys. Rev. Lett. **108**, 096404 (2012).
[30] G. Bian, T. Miller, and T. C. Chiang, Phys. Rev. Lett. **107**, 036802 (2011).
[31] G. Bian, T. Miller, and T.-C. Chiang, Europhys. Lett. **101**, 27004 (2013).
[32] G. Bian, X. Wang, Y. Liu, T. Miller, and T.-C. Chiang, Phys. Rev. B **84**, 235414 (2011).